NANO LETTERS

2009
Vol. 9, No. 12
4250-4257

Visible to Near-Infrared Light Harvesting in TiO_2 Nanotube Array−P3HT Based Heterojunction Solar Cells

Gopal K. Mor, Sanghoon Kim, Maggie Paulose, Oomman K. Varghese, Karthik Shankar,† James Basham, and Craig A. Grimes*

Department of Electrical Engineering, The Materials Research Institute, and Center for Solar Nanomaterials, The Pennsylvania State University, University Park, Pennsylvania 16802

Received July 31, 2009; Revised Manuscript Received September 11, 2009

ABSTRACT

The development of high-efficiency solid-state excitonic photovoltaic solar cells compatible with solution processing techniques is a research area of intense interest, with the poor optical harvesting in the red and near-IR (NIR) portion of the solar spectrum a significant limitation to device performance. Herein we present a solid-state solar cell design, consisting of TiO_2 nanotube arrays vertically oriented from the FTO-coated glass substrate, sensitized with unsymmetrical squaraine dye (SQ-1) that absorbs in the red and NIR portion of solar spectrum, and which are uniformly infiltrated with p-type regioregular poly(3-hexylthiophene-2,5-diyl) (P3HT) that absorbs higher energy photons. Our solid-state solar cells exhibit broad, near-UV to NIR, spectral response with external quantum yields of up to 65%. Under UV filtered AM 1.5G of 90 mW/cm^2 intensity we achieve typical device photoconversion efficiencies of 3.2%, with champion device efficiencies of 3.8%.

The best performing bulk heterojunction solar cells ($\eta \sim 6\%$) employ an optimized blend of a polymeric donor and a fullerene acceptor.[1,2] The fullerene acceptor absorbs very little light and is primarily used in blends to provide an efficient interface for exciton dissociation. Various efforts toward efficiency improvement in these devices are directed toward the development of low band gap polymers to absorb a broad swathe of the solar spectrum,[3−6] lowering the molecular energy levels of the semiconducting polymer to enhance the open circuit voltage of the organic solar cells,[1,7] and the control of the blended film morphology for enhanced exciton harvesting.[8−12] In the best performing solid-state dye-sensitized solar cells (SS-DSSCs), $\eta \sim 5\%$, the only photon absorber is a dye, while the electron and hole transport functions are performed, respectively, by a disordered nanoparticulate TiO_2 network and a transparent small molecule spiro-OMeTAD.[13−16] To achieve higher efficiency devices, research efforts have focused on improved pore-filling by the hole transporter, the use of higher mobility hole transporters and the synthesis of dyes with a broader and more-intense absorption spectrum.

Red/NIR radiation (650−1000 nm) accounts for approximately 33% of the solar energy arriving at the surface of the Earth, while UV−visible radiation (350−650 nm) accounts for about 40%. Hence a key issue toward achieving higher efficiency organic solar cells is in the development of red and NIR absorbing molecules to utilize more of the solar spectrum. As an approach for efficiently utilizing visible to NIR solar radiation, herein we describe an inorganic−organic hybrid solar cell, see Figure 1a, where electron transporting TiO_2 nanotube arrays, sensitized with red and NIR light absorbing organic dye, are used in combination with hole transporting and visible light absorbing regioregular P3HT.[17−19] It should be noted that this low band gap organic dye should not block transmission of the high-energy photons of near-UV−visible range passing through it; that is, the organic dye should have minimum spectral absorption overlap with that of the P3HT. As shown in Figure 1b, the position of the highest occupied molecular orbital (HOMO) and the lowest unoccupied molecular orbital (LUMO) levels for both organic dye and P3HT polymer should be such that electron injection is favorable toward TiO_2 while hole transport is directed toward the gold electrode. In our device, excited states generated in the dye find themselves in close proximity to two interfaces for dissociation: the TiO_2−dye interface and the dye−P3HT interface. For excitons generated in the P3HT, the P3HT−dye interface is the closest available for splitting and the largest distance the excitons need to diffuse to reach this interface corresponds to the radius of the nanotube pore. After exciton splitting, electrons are injected into the TiO_2, while hole−polarons travel through the P3HT layer to the PEDOT:PSS hole collection contact. The open circuit voltage V_{oc} is

* Corresponding author, cgrimes@engr.psu.edu.
† Current address: Department of Electrical and Computer Engineering, The University of Alberta, Edmonton, Alberta T6G 2 V4, Canada.

10.1021/nl9024853 CCC: $40.75
Published on Web 09/23/2009

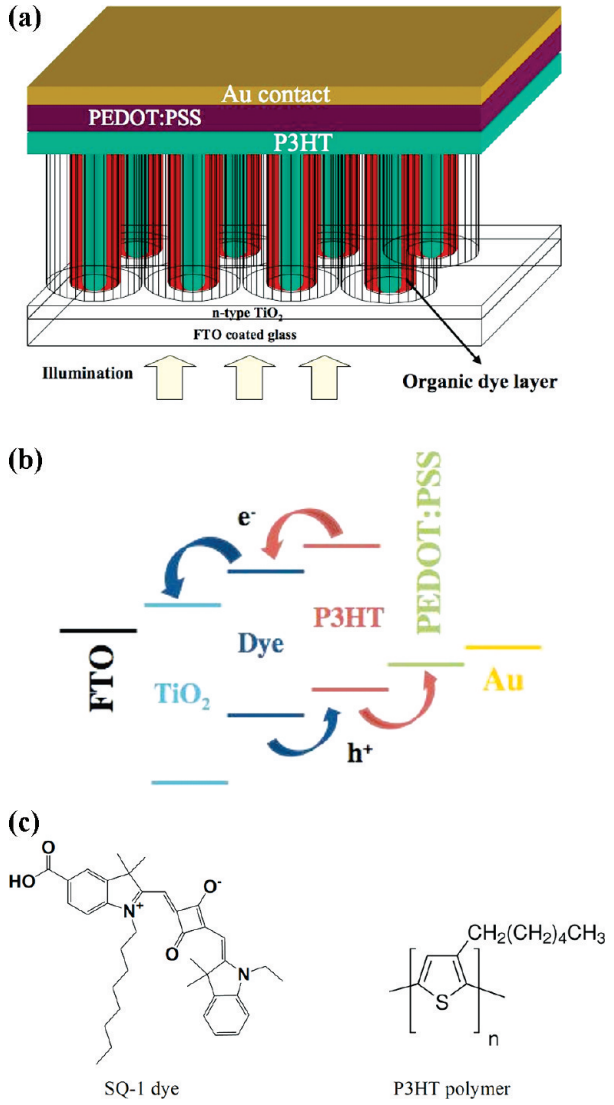

Figure 1. (a) Depiction of hybrid solid-state solar cell described herein. Dye sensitization and polymer intercalation between the nanotubes is not shown to maintain clarity of the drawing. (b) Depiction of energy level positions and charge transfer processes of the constituent layers of the described hybrid solar cell. (c) Molecular structure of SQ-1 dye and P3HT polymer.

determined by the TiO_2 quasi-Fermi level and the P3HT HOMO level. The TiO_2 nanotube array pore size, 20−35 nm, was selected such that P3HT chains can infiltrate into the pores but also allow photogenerated excitons in the P3HT to readily diffuse to the exciton splitting interface.

Our SS−DSSC configuration has the following key advantages: (i) The ordered heterojunction architecture provides percolation paths for both types of charge carriers.[12,20,21] (ii) The vertically oriented nanotube array architecture decouples exciton diffusion from light absorption.[22] (iii) There are two complementary photon absorbers that provide broad-spectrum absorption, namely, the dye molecules anchored to the nanotube walls and the organic semiconductor, in our case P3HT, within the nanotubes. High-quality organic−inorganic interfaces are typically difficult to achieve since inorganic materials, in our case TiO_2, are hydrophilic whereas commonly used semiconducting polymers, for example P3HT, with its large alkyl groups and uncharged backbone are hydrophobic. Likewise, the appropriate matching of the energy levels of a three-component system (inorganic n-type backbone, dye, hole transport material) and the creation of embedded exciton splitting interfaces is not trivial. Due to these difficulties, previous efforts by a number of researchers have focused on modifying the inorganic metal oxide surface by binding to it various organic molecules and ruthenium-based dyes that, in combination with hole transporting conjugated polymers, result in photovoltaic devices with photoconversion efficiencies well below 1%.[23−31] Here, we successfully demonstrate a device structure comprised of TiO_2 nanotube arrays/organic-dye/P3HT, with the vertically oriented TiO_2 nanotube arrays of small pore size providing a large interfacial surface area for dye adsorption and a large interfacial area between the organic dye monolayer and the P3HT. The successful infiltration of P3HT into the nanotube arrays is demonstrated.

We consider application of the organic dye, 5-carboxyl-2-[[3-[(1,3-dihydro-3,3-dimethyl-1-ethyl-2*H*-indol-2-ylidene)-methyl]-2-hydroxy-4-oxo-2-cyclobuten-1-ylidene] methyl]-3,3-trimethyl-1-octyl-3*H*-indolium (unsymmetrical squaraine, SQ-1).[32] The molecular structures of the SQ-1 dye and P3HT polymer are shown in Figure 1c. Synthesis details of SQ-1 are found in ref 32. The molecular design of dye SQ-1 is such that the carboxylic acid group is part of the conjugated π-system of the dye providing strong electronic coupling to the TiO_2 conduction band while the asymmetry created by the octyl chain prevents surface aggregation and limits self-quenching of the excited state.[33] The dye provides strong conjugation across the chromophore and anchoring group, enabling electronic coupling between the LUMO of the dye and TiO_2 conduction band. The absorption spectra of 0.1 mM SQ-1 dye dissolved in ethanol solution, see Figure 2a, indicates that SQ-1 absorbs from 500 to 700 nm with an extinction coefficient of 159700 M^{-1} cm^{-1} at λ_{max} of 637 nm corresponding to $\pi-\pi^*$ charge transfer transitions.

As shown in Figure 2b the absorption bands of SQ-1 dye and P3HT complement each other making the two materials appropriate for an extended spectrum solar cell, with the TiO_2 nanotubes, band gap 3.2 eV, absorbing the UV portion of the solar spectrum. The SQ-1 absorption peak observed in ethanol solution broadens with sensitization, 2 mM ethanol dye solution, on the TiO_2 nanotube arrays, Figure 2a. There is a small red shift of 9 nm in the peak position for SQ-1 suggesting J-type aggregation, which can further extend the photon absorption into the NIR region. P3HT coverage of the TiO_2 nanotube arrays shows no shift in the absorption peak position compared to that of neat P3HT films,[34] indicating a high degree of $\pi-\pi$ stacking of the polymer chains within the nanotubes. The spectral properties of the SQ-1 dye in ethanol solution and cyclic voltammetry determined electrochemical properties of the sensitizers upon the TiO_2 nanotube arrays are summarized in Table 1.

Electron−hole transfer processes occurring within the hybrid solid-state solar cell are depicted in Figure 1b. The LUMO level of the organic dye is more negative than the P3HT LUMO level and less negative than the TiO_2 conduction

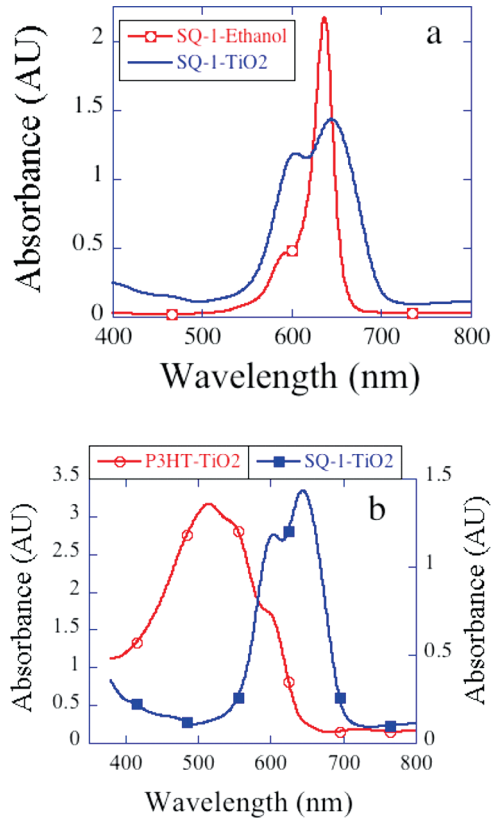

Figure 2. (a) Absorption spectra of SQ-1 dye in ethanol, and SQ-1 dye sensitized TiO_2 nanotube arrays exhibiting absorption peak broadening. (b) Optical absorbance of SQ-1 sensitized TiO_2 nanotube arrays and P3HT intercalated nanotube arrays without dye sensitization. The nanotube arrays had an average pore size of 35 nm and tube length of 600−700 nm.

band, Table 1. The HOMO level of the dye is close to or slightly below the HOMO level of P3HT. Hence upon absorption of a red/NIR photon the organic dye injects an electron into the TiO_2 conduction band and is regenerated by hole donation to the P3HT. Excitons generated in the P3HT dissociate into electrons and holes at the dye−P3HT interface, with the electrons passing to the dye layer/TiO_2, and the holes passing along P3HT chains to the PEDOT:PSS hole transport layer[35] and then to the gold electrode. Finally, we note that despite the success of the PEDOT−PSS blends, it has been shown that the presence of the strongly acidic and hygroscopic PSS can sometimes degrade device lifetime and performance.[36,37] The use of asymmetrical contacts (low work-function FTO and TiO_2 for electron collection, high work-function PEDOT:PSS and gold for hole collection) creates an external field under short circuit condition.[38] The gradient in the chemical potentials at the P3HT−organic dye interface should facilitate movement of the charge carriers to their respective electrodes.

We investigated the utility of TiO_2 nanotube arrays, on FTO coated glass substrates, having three different average pore sizes, of 20 nm (length ∼500 nm), 35 nm (length ∼600 to 700 nm) and 60 nm (length ∼1 to 1.2 μm).[39−41] All samples were crystallized and treated with aqueous $TiCl_4$ solution under identical conditions. A cross-sectional FESEM view of a $TiCl_4$ treated nanotube array film (length ∼1 to 1.2 μm) is shown in Figure 3a. We note that McGehee has advocated the usefulness of such an ordered architecture in a P3HT−mesoporous TiO_2 based system,[42] while Coakley and co-workers demonstrated infiltration of P3HT within nanoporous alumina using a high-temperature polymer melt-infiltration technique.[43] The nanotubes have the general shape of a common laboratory test tube, with the top of the tube open and the bottom closed.[44,45] To assist polymer infiltration within the tubes, the nanotube array film was wetted with *p*-xylene, a nonpolar organic solvent. After the excess solvent was removed, nanotube array films were then covered with a P3HT polymer solution (30 mg/mL concentration) prepared in a 3:1 mixture of *o*-dichlorobenzene (*o*-DCB) and chlorobenzene (CB). The sample was then spun, with the *p*-xylene acting to wick the P3HT inside the nanotube arrays and the polymer solution forming a thin layer atop the nanotube array film. The sample was then immediately transferred onto a 150 °C hot plate, with the remaining organic solvent quickly evaporating and the polymer inside the nanotubes making a dry interface with the dye molecule layer. After the sample was cooled to room temperature, a thin layer of PEDOT:PSS was spun onto the sample. It was then baked at 120 °C to remove water present in the PEDOT:PSS layer, avoiding degradation of the P3HT, and then finally at 150 °C to promote adhesion between the PEDOT:PSS and P3HT layers.

The spin-coating duration, used to control the wetting of the P3HT solution on the dye-sensitized TiO_2 nanotube arrays, is dependent on the following factors: type of glovebox used, circulation within the glovebox, and the (inert gas) pressure inside the glovebox when fabricating the sample. Hence instead of specifying the exact duration of spinning, we describe what we observe on the surface of the sample after we stop the sample spinning. After the suggested initial treatment with p-xylene on the dye-sensitized TiO_2 nanotube arrays was performed, we completely cover the sample surface with P3HT solution (30 mg/mL, 3:1 ratio *o*-DCB and CB) and start spinning the sample at 250 rpm. After the sample was spun for 200−300 s, we observe an excessively wet P3HT layer on top of the nanotube array film. Immediately transferring this sample to a 150 °C hot plate for 20 min, partial infiltration of the polymer is achieved due to evaporation of the *o*-DCB solvent; a cross-sectional image of such a sample with a PEDOT:PSS layer deposited on top is shown in Figure 3b. Extending the spinning time to 350−400 s, the resulting P3HT film is partially wet, our so-called optimized wetness condition. Hot plate baking of the sample results in uniform polymer intercalation within the nanotube arrays; see Figure 3c. With further extended spinning durations, 450−500 s, the P3HT layer dries, with only partial polymer decoration of the nanotubes obtained; see Figure 3d. The glancing angle X-ray diffraction (GAXRD) pattern, see Figure 4, of the completed device shows the presence of highly crystalline P3HT, where the peak at $2\theta = 5°$ corresponds to a P3HT interchain spacing associated with interdigitated alkyl chains.[46,47]

Details of the device structure, and hence performance, are dependent on the device fabrication procedure. Consider

Table 1. Absorption, Emission, and Electrochemical Properties of SQ-1 Dye and P3HT Polymer

dye/polymer	λ_{abs}[a], nm (ε, M^{-1} cm^{-1})	λ_{em}[a], nm	E_{ox}[b]/[V vs Fc/Fc$^+$]	E_{0-0}[c] (eV)	E_{HOMO}[d] (eV)	E_{LUMO}[d] (eV)
SQ-1 dye	637 (159700)	652	0.38	1.93	5.18	3.25
P3HT polymer[e]	443	568		1.9	5.1	3.2

[a] Absorption and emission spectra were measured in ethanol solution. [b] A silver wire was used as a pseudoreference electrode and was calibrated with a ferrocene/ferrocinium (Fc/Fc$^+$) redox couple. The electrochemical experiments were measured in CH_3CN with 0.1 M $(n\text{-}C_4H_9)_4NPF_6$ with a scan rate of 100 mV s^{-1}. [c] E_{0-0} was determined from intersection of absorption and emission spectra in ethanol. [d] The energy levels of the HOMO and LUMO were determined using the following equations: E_{HOMO} (eV) = $E_{ox} - E_{FC/FC^+} + 4.8$ eV; E_{LUMO} (eV) = $E_{HOMO} - E_{0-0}$. [e] P3HT polymer (average molecular weight ~50000 M_w) was dissolved in toluene for absorption and emission spectra, values given in the product information from Sigma Aldrich.

as an illustration the incident photon to collected electron efficiency (IPCE) of three of the described P3HT/dye-sensitized TiO_2 nanotube array devices, see Figure 5, with the P3HT solution (30 mg/mL, prepared using a 3:1 ratio of *o*-DCB and CB) applied in varying degrees of sample surface wetting as discussed in the preceding paragraph. Optimal samples exhibit an IPCE of 50−65% between 420 and 680 nm. The resulting samples appear reddish with a light violet tinge. Due to significant overlap between the emission spectrum of RR-P3HT and the absorption spectrum of the SQ-1 dye, exciton transfer from P3HT to the dye by Förster-type resonance energy transfer (FRET) is possible.[48−53] Upon calculating the spectral overlap integral from the normalized photoluminescence (of P3HT on a very thin TiO_2 film)[50] and absorption (of SQ-1 dye ethanolic solution) spectra, considering an emission quantum efficiency of 1% for P3HT,[51] and assuming random orientation of the donor and acceptor molecules and the effective refractive index of P3HT−TiO_2 film of 1.6, we calculate a Förster radius[48] of 2.58 nm which could result in an effective exciton diffusion length in the range 14−18 nm.[52,53] On the basis of exciton harvesting calculations given by Scully and co-workers,[53] it was found that about 65−75% of the excitons generated in P3HT infiltrated inside 35 nm pore size TiO_2 nanotube arrays can be harvested. The coexistence of resonance energy transfer may account for the high charge transfer efficiencies in this system as inferred from external quantum yield measurements. A detailed analysis of the energy transfer efficiency and of the relative contributions of exciton transfer and exciton quenching at the dye−P3HT interface is in progress.

We initially investigated the utility of three different TiO_2 nanotube array morphologies having dimensions: (i) pore size ~20 nm and length ~500 nm; (ii) pore size ~35 nm and length 600−700 nm; (iii) pore size 60 nm and length ~1−1.2 μm. Figure 6a shows the UV−vis−NIR absorption spectra of SQ-1 dye sensitized nanotube arrays, with significantly greater absorption seen for the nanotubes of 35 and 60 nm pore diameters. Figure 6b shows the UV−vis−NIR optical absorption spectra of typical TiO_2 nanotube (35 nm pore, 600−700 nm length)/SQ-1 dye/ P3HT/PEDOT:PSS photovoltaic device fabricated under optimized wetting condition. The absorption peak corresponding to P3HT indicates a high degree of $\pi-\pi$ polymer chain stacking. We have seen no shift in the P3HT absorption peak position as a function of nanotube pore size. The $J-V$ characteristics of three TiO_2 nanotube/SQ-1/P3HT/PEDOT:PSS devices, variable nanotube array dimensions, are shown in Figure 7a. As anticipated, the 20 and 35 nm pore size nanotubes give larger fill factors and higher current values, while it was significantly easier to infiltrate P3HT within the 35 and 60 nm pore nanotubes. On the basis of the amount of SQ-1 dye adsorbed by the three different samples, Figure 6a, and the saturated photocurrent values, Figure 7a, the 35 nm pore size nanotube arrays appeared optimal for device fabrication.

We further improved the fill factor and open-circuit voltage of the SQ-1 dye based solar cells by wetting the SQ-1 sensitized nanotube array films (pore size ~35 nm, tube length 600−700 nm) with 0.05−0.1 M *tert*-butyl pyridine in *p*-xylene solution (instead of pure *p*-xylene), spin coating the P3HT and PEDOT:PSS layers, depositing the gold electrode, and then baking the device at 120 °C for 1 min in air. The performance of a typical device is shown in Figure 7b, with $J_{sc} = 10.75$ mA/cm^2, $V_{oc} = 0.55$ V, $FF = 0.55$. and $\eta = 3.2\%$. *tert*-Butylpyridine is known to increase the open circuit voltage by upward shifting the TiO_2 band edge[54,55] and by physically sealing molecular scale voids at the interface. The efficiency of our champion device was found to be 3.8% ($J_{sc} = 11$ mA/cm^2, $V_{oc} = 0.6$ V, $FF = 0.58$). If we account for the transmittance loss of 10% across the visible range due to the UV filter in the light source (necessary since UV light rapidly degrades the SQ-1 dye), an efficiency of $\approx 4.2\%$ can be expected.

Figure 7b also shows the performance of a typical TiO_2 nanotube array/P3HT (no organic dye) solar cell, having key device parameters $J_{sc} = 1.8$ mA/cm^2, $V_{oc} = 0.41$ V, $FF = 0.46$, and $\eta = 0.34\%$. With use of the organic dye layer the photoconversion efficiency of a typical device increases from 0.34% to 3.2%, with the open circuit voltage increasing from 0.41 to 0.55 V. Acid−base interactions arising from carboxylic group anchoring of the organic dye affect the TiO_2 band edge by protonating it. As reported by Goh and co-workers,[28] the magnitude of this shift is about 0.2 eV for Ru(II) dyes. We note that extensive $TiCl_4$ treatment of the nanotubes was found to increase the open-circuit voltage to 0.67 V but resulted in considerably lower photocurrents. The $J-V$ and IPCE measurements of our devices were performed in air. Though we did not perform any long-term stability tests, the photovoltaic results were consistent for a number of runs made over several days. The cell surface area is defined by removal of the PEDOT:PSS layer around the circular gold electrode before all electrical measurements, thereby exposing the underlying P3HT polymer to ambient air; hence it is not appropriate to comment on the long-term stability of these samples.

Ordered heterojunction solar cells based on TiO_2 nanotube arrays sensitized by a red/NIR absorbing organic dye in combination with a hole transporting organic semiconductor is an exciting photovoltaic design since it combines the attractive features of both solid-state dye-sensitized solar cells and bulk heterojunction solar cells, while overcoming some

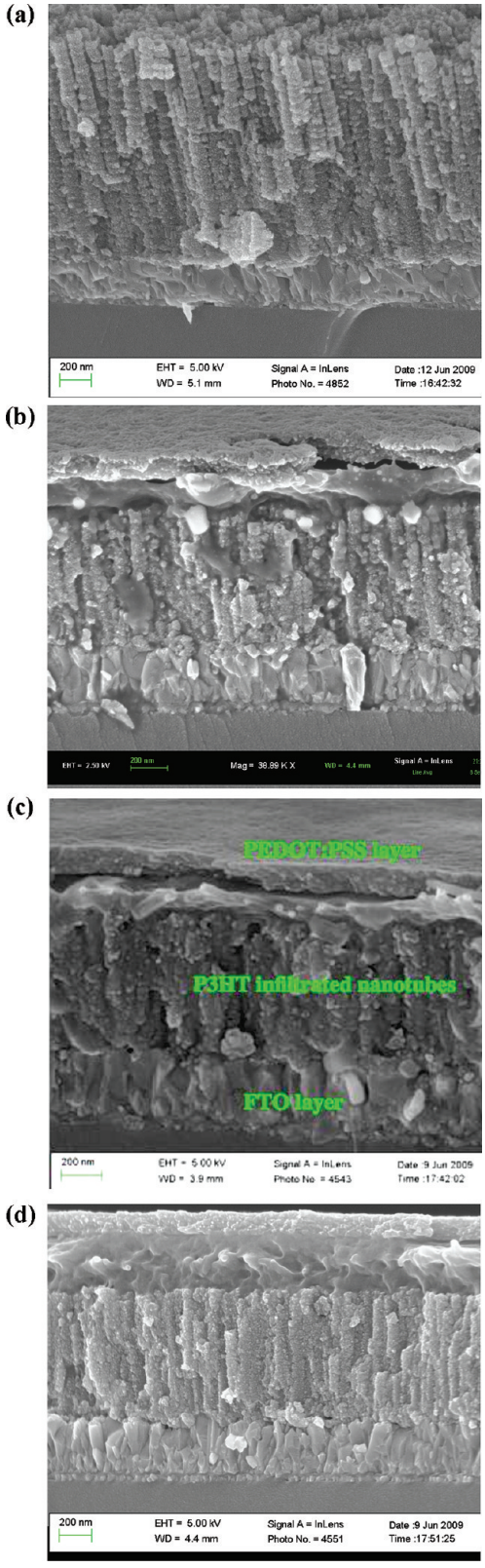

Figure 3. (a) Typical cross-sectional view of 60 nm pore size, 1−1.2 μm length TiO_2 nanotube array film after $TiCl_4$ treatment. Cross-sectional FESEM image of TiO_2 nanotube (≈35 nm pore size, ≈600−700 nm nanotube length)/SQ-1 dye/P3HT/PEDOT:PSS photovoltaic devices showing: (b) nanotubes partially infiltrated with polymer, fabricated under the condition of excess wetness; (c) fully infiltrated nanotubes fabricated under optimized wetness condition; and (d) partial infiltration of the P3HT polymer within the nanotubes, fabricated under dry condition.

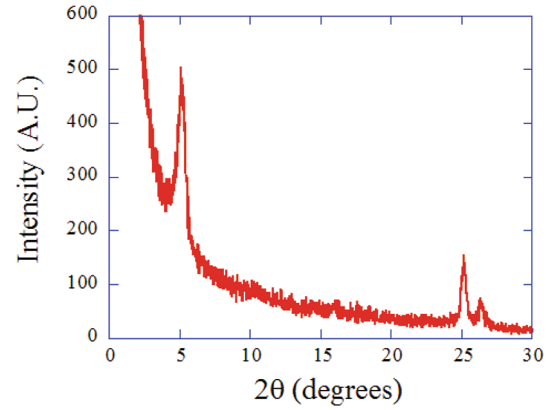

Figure 4. GAXRD pattern of the actual completed device, FTO/TiO_2 nanotube array/SQ-1 dye/P3HT/PEDOT:PSS. The peak at $2\theta = 5°$ corresponds to a P3HT interchain spacing associated with interdigitated alkyl chains, the peak at $2\theta = 25.2°$ arises from anatase phase of TiO_2, and the peak at $2\theta = 26.4°$ is from the FTO coating. We could not find a peak corresponding to PEDOT:PSS due to its small thickness.

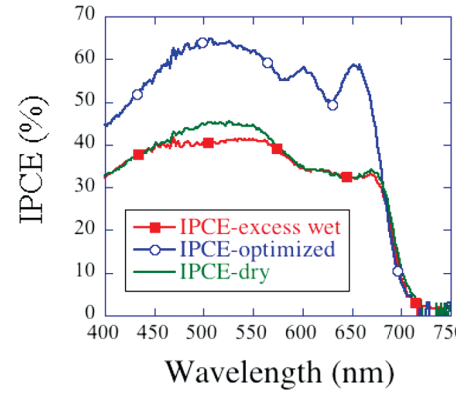

Figure 5. IPCE of a FTO/TiO_2 nanotube array/SQ-1 dye/P3HT/PEDOT:PSS/Au solar cell, where the P3HT layer was prepared with different degrees of surface wetness prior to a 150 °C postbake. Excess wetness, where the film was still wet entering the postbake; optimized, where upon just visually drying the device was immediately removed from the spinner and exposed to the postbake; dry, indicating where the film had dried on the spinner prior to postbake. The dye sensitization and PEDOT:PSS layer are identical in all the three samples. Nanotube array films of 35 nm average pore diameter and 600−700 nm length were used.

of the limitations of the established configurations. We demonstrate that this device structure offers a potentially viable means for achieving high efficiency low cost solid-state solar cells. Our devices achieve high photocurrents due to the contribution of two photoactive layers, the organic dye monolayer and P3HT polymer. Moreover, the conjugated polymer chains infiltrated inside the vertically oriented TiO_2 nanotube arrays appear to be aligned, see Figure 4, resulting in enhanced carrier mobilities.[43] Our device architecture suggests further opportunities exist for extended light harvesting, and improvement in the open circuit voltage, by tailoring the TiO_2 surface to raise the conduction band position or using other p-type polymers where the HOMO level positions appear to be more negative with respect to that of P3HT but still sufficient for regeneration of the organic dye.

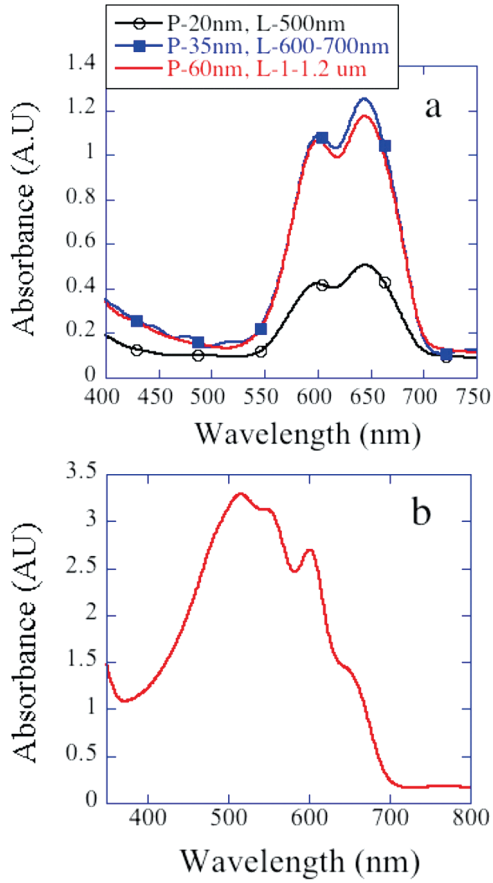

Figure 6. (a) UV−vis−NIR optical absorption spectra of SQ-1 dye sensitized TiO_2 nanotube arrays of three different morphologies (P denotes pore diameter, L denotes nanotubes length). The absorption peak magnitude corresponding to SQ-1 dye is nearly the same for the 35 and 60 nm pore size nanotubes, which is much higher than that of the 20 nm pore size nanotubes. (b) UV−vis−NIR optical absorption spectra of typical TiO_2 nanotube/SQ-1 dye/ P3HT/PEDOT:PSS photovoltaic device fabricated under optimized wetting condition. The absorption peak corresponding to P3HT indicates a high degree of $\pi-\pi$ polymer chain stacking. We have seen no shift in the P3HT absorption peak position as a function of nanotube pore size.

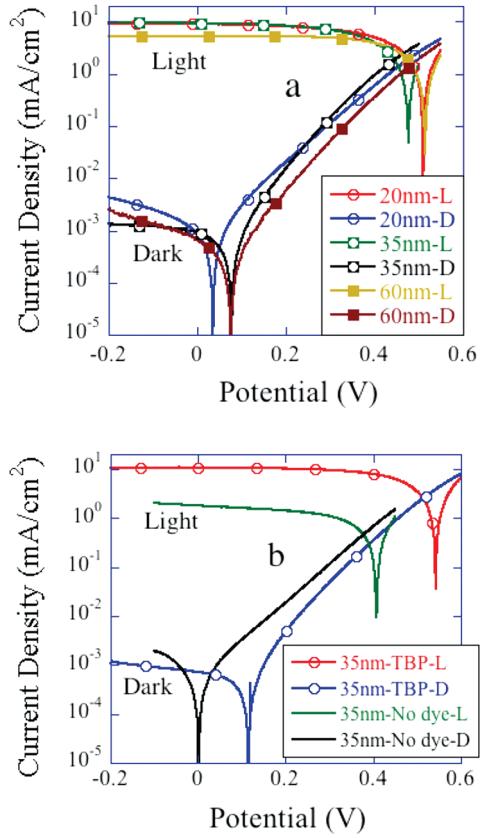

Figure 7. (a) Photocurrent density−voltage ($J-V$) characteristics of FTO/TiO_2 nanotube array/SQ-1 dye /P3HT/PEDOT:PSS/Au hybrid solar cells using nanotube arrays of three different morphologies: 20 nm pore and ≈500 nm length; 35 nm pore and ≈600−700 nm length; 60 nm pore and ≈1−1.2 μm length. The 35 nm pore nanotube arrays were found to give optimal solar cell performance. (b) $J-V$ curves showing the improved performance of a FTO/35 nm pore, 600−700 nm length TiO_2 nanotube array/ SQ-1 dye/P3HT/PEDOT:PSS/Au hybrid solar cell where the dye-sensitized nanotube array surface, prior to application of the P3HT layer, is wetted with 0.05−0.1 M *tert*-butyl pyridine in *p*-xylene. Also shown is the performance of an otherwise identical cell lacking the SQ-1 dye layer. *L* denotes measurement under AM 1.5G light, *D* denotes measurement in the dark.

Methods. ***Device Fabrication.*** Details on fabrication of the transparent nanotube array films are given elsewhere.[39] In short, Ti films were deposited using rf or dc magnetron sputtering of titanium targets on Pilkington TEC 15 glass (sheet resistance 15 Ω/square) substrates in argon atmosphere. No external heating was applied to the substrates. The films were anodized in an electrolyte consisting of dimethyl sulfoxide (DMSO), 2−4% hydrofluoric acid (HF), and 4% water at voltages from 8 to 17 V until transparency was achieved. The films were washed in isopropanol and dried in a nitrogen stream. The samples were subjected to heat treatment in an oxygen atmosphere at 400 °C for 4 h and then at 450 °C for 2 h with a ramp-up and ramp-down rate of 1 °C/min. The films were then immersed in 0.05 M $TiCl_4$ aqueous solution for 6 h, then rinsed with ethanol and distilled water, dried in air, and then annealed at 450 °C for 30 min in oxygen. After the samples had cooled to 80 °C, they were immersed in 2.0 mM SQ-1 dye solution prepared in ethanol.

The dye-sensitized samples were transferred into a nitrogen-filled glovebox (MBraun, MB 150M) where they were baked at 120 °C for 10 min and then upon cooling transferred onto the spin coater. To assist polymer infiltration within the tubes, the nanotube array film was wetted with *p*-xylene with excess solvent removed by sample rotation on a spin coater. Immediately following, the nanotube array surface was covered with a P3HT polymer (Rieke Metals, Inc.) solution (30 mg/mL concentration) prepared in a 3:1 mixture of *o*-dichlorobenzene (*o*-DCB, boiling point ∼180.5 °C) and chlorobenzene (CB, boiling point ∼131 °C). The sample was then spun at 250 rpm, with the *p*-xylene facilitating intercalation of the P3HT inside the nanotube arrays and the polymer solution forming a thin layer atop the nanotube array film. Spinning was stopped just before the polymer layer over the surface of the nanotubes dried, typically about 10 min. The sample was then immediately transferred onto a 150 °C hot plate for 20 min. After the sample was allowed to cool to room temperature, a thin layer of PEDOT:PSS (1.2−1.7 wt

% dispersion in water, Sigma Aldrich) was spun onto the sample at 4000 rpm. After this, the samples were baked at 120 °C for 6 min and then at 150 °C for 3 min. Finally, a circular gold electrode was dc sputter deposited onto the PEDOT:PSS film through a mask containing 2 mm diameter circular openings, followed by a final baking of the sample at 120 °C for 1 min in covered glass Petri dish. The PEDOT:PSS layer around the gold electrode was cut away prior to any electrical measurements.

Electrical Characterization. Device efficiencies were measured with a 500 W Spectra Physics light source fitted with Oriel AM 1.5G filter. The solar simulator was calibrated for AM 1.5G illumination using an NREL calibrated silicon solar cell fitted with a KG-5 filter (Newport M465440). The irradiance spectrum was verified using an optical spectrometer (Newport, OSM2-400DUV-U). After calibration, a UV filter (Edmund optics, NT54) was installed that removed light below 380 nm and reduced the light intensity from 400 to 800 nm by about 10% to 90 mW/cm^2. A scanning potentiostat (CH Instruments, CHI 600C) was used to measure photocurrents at a scan rate of 10 mV/s. $J-V$ measurements were not corrected for any of this optical intensity loss. IPCE spectra measurements were performed using a 300 W xenon lamp (Spectra physics), integrated with a parabolic reflector, and computer-controlled monochromator (Oriel Cornerstone 130, 1/8 monochromator). The source power spectrum was measured using an Oriel calibrated silicon photodiode (model 71580). The photocurrent measurement scan was from lower to higher wavelengths.

Optical, Structural, and Morphology Characterization. UV−vis absorption spectra and photoluminescence spectra of SQ-1 dye in ethanol were measured, respectively, on a UV−vis spectrophotometer (Varian Cary 100) and Fluorolog 3-21 spectrophotometer (Horiba Jobin Yvon, Edison, NJ). Illustrative cross-sectional and top views of polymer infiltrated TiO_2 nanotubes and $TiCl_4$ treated nanotubes were taken using a field emission scanning electron microscope (LEO 1530 FESEM). GAXRD analysis was performed using a Scintag X2 diffractometer (Scintag Inc., CA).

Electrochemistry. All electrochemical measurements were performed in *acetonitrile* with 1.0 mM tetra-*n*-butylammonium hexafluorophosphate (*n*-Bu_4NPF_6, Aldrich, ~99%), as supporting electrolyte. Cyclic voltammetry experiments were performed using a potentiostat (CH Instruments, model CHI 600C) with a standard three-electrode arrangement. The working electrode consisted of SQ-1 dye sensitized TiO_2 nanotube array films. A silver wire served as a pseudoreference electrode. Ferrocene was added to the solution at the end of each experiment as an internal standard, and then a glassy carbon disk (1 mm diameter, ESA Biosciences) was used as the working electrode. All the electrochemical potentials were referenced to its redox couple (Fc/Fc+). The counter electrode employed was a platinum wire.

Acknowledgment. Support of this work through the Department of Energy, Grant Number DE-FG36-08GO18074, is gratefully acknowledged, as is the help of Thomas LaTempa with the GAXRD measurements.

References

(1) Park, S. H.; Roy, A.; Beaupre, S.; Cho, S.; Coates, N.; Moon, J. S.; Moses, D.; Leclerc, M.; Lee, K.; Heeger, A. J. *Nat. Photonics* **2009**, *3*, 297–303.
(2) Liang, Y.; Feng, D.; Wu, Y.; Tsai, S. T.; Li, G.; Ray, C.; Yu, L. *J. Am. Chem. Soc.* **2009**, *131*, 7792–7799.
(3) Tamayo, A. B.; Dang, X. D.; Walker, B.; Seo, J.; Kent, T.; Nguyen, T. Q. *Appl. Phys. Lett.* **2009**, *94*, 103301.
(4) Liang, Y.; Wu, Y.; Feng, D.; Tsai, S. T.; Son, H. J.; Li, G.; Yu, L. *J. Am. Chem. Soc.* **2009**, *131*, 56–57.
(5) Cho, S.; Seo, J. H.; Kim, S. H.; Song, S.; Jin, Y.; Lee, K.; Suh, H.; Heeger, A. J. *Appl. Phys. Lett.* **2008**, *93*, 263301.
(6) Wang, X.; Perzon, E.; Delgado, J. L.; de la Cruz, P. *Appl. Phys. Lett.* **2004**, *85*, 5081–5083.
(7) Blouin, N.; Michaud, A.; Gendron, D.; Wakim, S.; Blair, E.; Neagu-Plesu, R.; Belletete, M.; Durocher, G.; Tao, Y.; Leclerc, M. *J. Am. Chem. Soc.* **2008**, *130*, 732–742.
(8) Moulé, A. J.; Meerholz, K. *Adv. Mater.* **2008**, *20*, 240–245.
(9) Vanlaeke, P.; Vanhoyland, G.; Aernouts, T.; Cheyns, D.; Deibel, C.; Manca, J.; Heremans, P.; Poortmans, J. *Thin Solid Films* **2006**, *511−512*, 358–361.
(10) Watkins, P. K.; Walker, A. B.; Verschoor, G. L. B. *Nano Lett.* **2005**, *5*, 1814–1818.
(11) Hoppe, H.; Niggemann, M.; Winder, C.; Kraut, J.; Hiesgen, R.; Hinsch, A.; Meissner, D.; Sariciftci, N. S. *Adv. Funct. Mater.* **2004**, *14*, 1005–1011.
(12) Mor, G. K.; Shankar, K.; Paulose, M.; Varghese, O. K.; Grimes, C. A. *Appl. Phys. Lett.* **2007**, *91*, 152111.
(13) Snaith, H. J.; Petrozza, A.; Ito, S.; Miura, H.; Gratzel, M. *Adv. Funct. Mater.* **2009**, *19*, 1810–1818.
(14) Snaith, H. J.; Humphry-Baker, R.; Chen, P.; Cesar, I.; Zakeeruddin, S. M.; Gratzel, M. *Nanotechnology* **2008**, *19*, 424003.
(15) Snaith, H. J.; Moule, A. J.; Klein, C.; Meerholz, K.; Friend, R. H.; Gratzel, M. *Nano Lett.* **2007**, *7*, 3372–3376.
(16) Campbell, W. M.; Jolley, K. W.; Wagner, P.; Wagner, K.; Walsh, P. J.; Gordon, K. C.; Schmidt-Mende, L.; Nazeeruddin, M. K.; Wang, Q.; Gratzel, M.; Officer, D. L. *J. Phys. Chem. C* **2007**, *111*, 11760–11762.
(17) Parkinson, P.; Hughes, J. L.; Johnston, M. B.; Herz, L. M. *Phys. Rev. B* **2008**, *78*, 115321.
(18) Sirringhaus, H.; Brown, P. J.; Friend, R. H.; Nielsen, M. M.; Bechgaard, K.; Langeveld-Voss, B. M. W.; Spiering, A. J. H.; Janssen, R. A. J.; Meijer, E. W.; Herwig, P.; de Leeuw, D. M. *Nature* **1999**, *401*, 685–688.
(19) Sirringhaus, H.; Tessler, N.; Friend, R. H. *Science* **1998**, *280*, 1741–1744.
(20) Shankar, K.; Bandara, J.; Paulose, M.; Wietasch, H.; Varghese, O. K.; Mor, G. K.; LaTempa, T. J.; Thelakkat, M.; Grimes, C. A. *Nano Lett.* **2008**, *8*, 1654–1659.
(21) Mor, G. K.; Shankar, K.; Paulose, M.; Varghese, O. K.; Grimes, C. A. *Nano Lett.* **2006**, *6*, 215–218.
(22) Ong, K. G.; Varghese, O. K.; Mor, G. K.; Shankar, K.; Grimes, C. A. *Sol. Energy Mater. Sol. Cells* **2007**, *91*, 250–257.
(23) Gebeyehu, D.; Brabec, C. J.; Sariciftci, N. S.; Vangeneugden, D.; Kiebooms, R.; Vanderzande, D.; Kienberger, F.; Schindler, H. *Synth. Met.* **2002**, *125*, 279–287.
(24) Sicot, L.; Fiorini, C.; Lorin, A.; Nunzi, J. M.; Raimond, P.; Sentein, C. *Synth. Met.* **1999**, *102*, 991–992.
(25) Beltran, E. L.; Prené, P.; Boscher, C.; Belleville, P.; Buvat, P.; Lambert, S.; Guillet, F.; Marcel, C.; Sanchez, C. *Eur. J. Inorg. Chem.* **2008**, 903–910.
(26) Zafer, C.; Karapire, C.; Sariciftci, N. S.; Icli, S. *Sol. Energy Mater. Sol. Cells* **2005**, *88*, 11–21.
(27) Li, B.; Wang, L.; Kang, B.; Wang, P.; Qiu, Y. *J. Photochem. Photobiol., A* **2005**, *172*, 135–139.
(28) Goh, C.; Scully, S. R.; McGehee, M. D. *J. Appl. Phys.* **2007**, *101*, 114503.
(29) Williams, S. S.; Hampton, M. J.; Gowrishankar, V.; Ding, I. K.; Templeton, J. L.; Samulski, E. T.; DeSimone, J. M.; McGehee, M. D. *Chem. Mater.* **2008**, *20*, 5229–5234.
(30) Murakoshi, K.; Kogure, R.; Wada, Y.; Yanagida, S. *Sol. Energy Mater. Sol. Cells* **1998**, *55*, 113–125.
(31) Kitamura, T.; Maitani, M.; Matsuda, M.; Wada, Y.; Yanagida, S. *Chem. Lett.* **2001**, 1054–1055.
(32) Yum, J. H.; Walter, P.; Huber, S.; Rentsch, D.; Geiger, T.; Nuesch, F.; Angelis, F. D.; Gratzel, M.; Nazeeruddin, M. K. *J. Am. Chem. Soc.* **2007**, *129*, 10320–10321.

(33) Ooyama, Y.; Harima, Y. *Eur. J. Org. Chem.* **2009**, 2903–2934.
(34) Coakley, K. M.; McGehee, M. D.*Chem. Mater.* **2004**, *16*, 4533–4542.
(35) Groenendaal, L.; Dhaen, J.; Manca, J.; Van Luppen, J.; Verdonck, E.; Louwet, F.; Leenders, L. *Synth. Met.* **2003**, *135*−*136*, 115–117.
(36) Kawano, K.; Pacios, R.; Poplavskyy, D.; Nelson, J.; Bradley, D.; Durrant, J. R. *Sol. Energy Mater. Sol. Cells* **2006**, *90*, 3520–3530.
(37) Danier Van Der Gon, A. W.; Birgerson, J.; Fahlman, M.; Salaneck, W. R. *Org. Electrochem.* **2002**, *3*, 111–118.
(38) Parker, I. D. *J. Appl. Phys.* **1994**, *75*, 1656–1666.
(39) Varghese, O. K.; Paulose, M.; Grimes, C. A. *Nat. Nanotechnol.* **2009**, *4*, 592–597.
(40) Mor, G. K.; Varghese, O. K.; Paulose, M.; Grimes, C. A. *Adv. Funct. Mater.* **2005**, *15*, 1291–1296.
(41) Mor, G. K.; Varghese, O. K.; Paulose, M.; Ong, K. G.; Grimes, C. A. *Thin Solid Films* **2006**, *496*, 42–48.
(42) McGehee, M. D. *MRS Bull.* **2009**, *34*, 95–100.
(43) Coakley, K. M.; Srinivasan, B. S.; Ziebarth, J. M.; Goh, C.; Liu, Y.; McGehee, M. D. *Adv. Funct. Mater.* **2005**, *15*, 1927–1932.
(44) Mor, G. K.; Varghese, O. K.; Paulose, M.; Shankar, K.; Grimes, C. A. *Sol. Energy Mater. Sol. Cells* **2006**, *90*, 2011–2075.
(45) Grimes, C. A.; Mor, G. K. *TiO_2 Nanotube Arrays: Synthesis, Properties, and Applications*; Springer: Berlin, 2009.
(46) Chen, T. A.; Wu, X.; Rieke, R. D. *J. Am. Chem. Soc.* **1995**, *117*, 233–244.
(47) Ma, W.; Yang, C.; Gong, X.; Lee, K.; Heeger, A. J. *Adv. Funct. Mater.* **2005**, *15*, 1617–1622.
(48) Forster, T. *Discuss. Faraday Soc.* **1959**, *27*, 7–17.
(49) Shankar, K.; Feng, X.; Grimes, C. A. *ACS Nano* **2009**, *3*, 788–794.
(50) Liu, Y.; Summers, M. A.; Edder, C.; Fréchet, J. M. J.; McGehee, M. D. *Adv. Mater.* **2005**, *17*, 2960–2964.
(51) Sheng, C. X.; Tong, M.; Singh, S.; Vardeny, Z. V. *Phys. Rev. B* **2007**, *75*, 085206.
(52) Scully, S. R.; McGehee, M. D. *J. Appl. Phys.* **2006**, *100*, 034907.
(53) Scully, S. R.; Armstrong, P. B.; Edder, C.; Fréchet, J. M. J.; McGehee, M. D. *Adv. Mater.* **2007**, *19*, 2961–2966.
(54) Haque, S. A.; Tachibana, Y.; Willis, R. L.; Moser, J. E.; Gratzel, M.; Klug, D. R.; Durrant, J. R. *J. Phys. Chem. B* **2000**, *104*, 538–547.
(55) Zhu, R.; Jiang, C. Y.; Liu, B.; Ramakrishna, S. *Adv. Mater.* **2009**, *21*, 994–1000.

NL9024853